



ELSEVIER

Contents lists available at [SciVerse ScienceDirect](http://www.sciencedirect.com)

Comptes Rendus Physique

www.sciencedirect.com

Use of large scale facilities for research in metallurgy

Atomic structure of bulk metallic glasses and their supercooled liquid states probed by high-energy synchrotron light

*La structure atomique des verres métalliques massifs et de leurs états de liquides surfondus sondée par diffraction de la lumière haute-énergie du synchrotron*K. Georgarakis^{a,b}, A.R. Yavari^{a,*}, D.V. Louzguine^b, G. Vaughan^c, W.J. Botta^d^a SIMAP-CNRS, institut polytechnique de Grenoble, BP 75, Saint-Martin-d'Hères campus, 38402 Saint-Martin-d'Hères, France^b WPI Advanced Institute for Materials Research, Tohoku University, Aoba-Ku, Sendai, Japan^c European Synchrotron Radiation Facility, Grenoble, France^d DeMa, Univ. Federal de Sao Carlos (UFSCar), SP, Brazil

ARTICLE INFO

Article history:

Available online 3 February 2012

Keywords:

Bulk metallic glasses
Atomic structure
Synchrotron light
Supercooled liquid

Mots-clés :

Verres métalliques massifs
Structure atomique
Lumière du synchrotron
Liquide surfondu

ABSTRACT

Like non-metallic glasses, many bulk metallic glasses manifest a glass-transition temperature T_g during heating prior to crystallisation. While the exact nature of the atomic structure of a metallic glass depends on its thermo-mechanical history (quench-rate, plastic deformation, ...), a unique and reproducible average atomic structure is attained if the glass transition temperature can be approached in a reversible manner. However, a metallic glass is always metastable and crystallises within a time t near or above its T_g in such a way that any reciprocal or real-space information on the fully glassy state at $T \geq T_g$ must be completed within acquisition times $\tau_a \ll t$ and this condition is in general difficult to attain with conventional X-ray diffraction devices.

Here we report on experiments using high-energy, high-flux synchrotron light in the transmission for probing of the atomic structure of bulk metallic glasses. Examples are given of the determination of the isochoric glass transition T_g and the quenched-in free-volume. Finally, we report on the evolution of the atomic structure in the supercooled liquid region ($T > T_g$) and its role in the enhancement of glass formability.

© 2011 Académie des sciences. Published by Elsevier Masson SAS. All rights reserved.

R É S U M É

Comme les verres classiques, de nombreux verres métalliques massifs manifestent une température de transition vitreuse T_g au cours du chauffage avant de se cristalliser. Si la nature exacte de la structure atomique d'un verre métallique dépend de son histoire thermo-mécanique (vitesse de trempe, la déformation plastique, ...), une unique et reproductible structure atomique moyenne est atteinte si la température de transition vitreuse peut être approchée de manière réversible. Toutefois, un verre métallique est toujours métastable et se cristallise dans un temps, t , au voisinage ou au-dessus de sa T_g de telle manière que toute l'information dans les espaces réciproque et réel sur l'état totalement vitreux à $T \geq T_g$ doit être obtenue dans des temps d'acquisition $\tau_a \ll t$ et cette condition est en général difficile à atteindre avec les dispositifs classiques de diffraction des rayons-X. Nous rapportons ici les expériences de diffraction de la lumière synchrotron de haute énergie en transmission pour sonder la structure atomique de verres

* Corresponding author.

E-mail address: yavari@minatec.inpg.fr (A.R. Yavari).

métalliques massifs. Des exemples sont donnés de la détermination de la transition vitreuse isochore T_g , la mesure du volume-libre d'excès piégé par la trempe. Nous présentons également l'évolution de la structure atomique dans la région du liquide sous-refroidi ($T > T_g$) et son rôle dans l'amélioration de la formabilité des verres métalliques.

© 2011 Académie des sciences. Published by Elsevier Masson SAS. All rights reserved.

1. Introduction

Metallic glasses are binary or multi-component alloys cooled from their liquid state without the formation of coherent domains (crystallisation) with periodic atomic long-range order [1].

Plastic deformation as in crystalline materials via dislocation motion on glide planes at very small fractions of the theoretical strength [2] is therefore inaccessible to metallic glasses leading to very high resilience with large elastic deformation [3–5] ranges $\varepsilon_{el} > 2\%$ prior to yielding. Their combination of unusual mechanical, electrochemical, tribological and magnetic properties is attractive from research and applications points of view. Their complex atomic structures, relations to their various physical properties and the technological applications of the latter are under intense study [6–9].

Recent investigations using state-of-the-art characterisation tools such as synchrotron radiation and computer simulations have improved our understanding of the atomic structure and its correlation with the properties of metallic glasses. In spite of their non-crystalline structure, the attractive interatomic interactions and the size differences between atomic species constituting a glassy alloy lead to short and medium-range orders characterised by clusters of atoms which connect to fill space as densely as their crystalline counterparts to within less than 2% [10–16].

The atomic structure of a monoatomic liquid metal can be approximately modelled by a dense random packing (DRP) of hard spheres resulting in space filling or packing density of about 64% [17]. This is to be compared with a packing density of 74% for a close-packed FCC structure. As a result of this difference, statistical atomic-level density fluctuations [18] in a monoatomic liquid below the melting temperature can easily form close-packed aggregates of atoms with crystalline order that can then grow quickly into stable nuclei and a monoatomic DRP cannot be quenched into a glassy state [19] except by computer simulation.

Near eutectic $\text{Au}_{80}\text{Si}_{20}$, $\text{Pd}_{80}\text{Si}_{20}$, and $\text{Fe}_{80}\text{B}_{20}$ binary liquid alloys were among the first to be quenched to a glassy state by rapid solidification at cooling rates greater than 10^5 K/s and thicknesses ≤ 50 μm [20,21]. Their glass-forming ability was explained by the smaller Si and B atoms “stuffing” the interstitial “holes” of the host atom DRP skeletons [22], a process that significantly increases the packing density and reduces what can be referred to as “structural” free-volume.

Additions of combinations of atoms of different sizes have since drastically improved ease of glass formation [1] and allowed relatively slow vitrification of multicomponent alloys with packing densities that are within about 1% of those of their crystalline states [23].

Increasing packing density slows the kinetics of atomic motion, increases viscosity and facilitates the suppression of nucleation and growth of crystalline phases [24,25] and the viscosity in the undercooled melt is the key material parameter in this process. Atomistically, this is due to an evolution from simpler DRP liquids to atomic structures that are complex packings of efficiently packed, quasi-stoichiometric clusters of atoms [10–16].

High glass-forming ability (GFA) achieved at some alloy compositions allows production of bulk metallic glasses in the thickness range of 1 mm to several cm by using various casting processes [1]. Pd–Ni–Cu–P bulk metallic glasses are the best glass-formers known to date. The Zr-rich Zr–Cu–Ni–Al family free of metalloid atom content is the next best glass-former.

In the present work we focus on some successful examples of application of high energy synchrotron light to study the atomic structure of multi-component Pd–Ni–Cu–P bulk metallic glasses at temperatures $T < T_g$ and their supercooled liquid state at $T > T_g$.

Three types of experiments are considered: the determination of the glass transition temperatures T_g and coefficients of thermal expansion α_{th} using monochromatised synchrotron light; measurement of the “quenched-in” or “excess free volume” V_f and finally possible evolutions of the nature of atomic bonding in the supercooled liquid region of a bulk metallic glass former.

2. Measuring the “isochoric” glass transition T_g

The isentropic glass transition T_g in metallic glasses [21–24] is measured by calorimetric techniques which show an endothermic event corresponding to a specific heat ΔC_p difference between the glassy and supercooled liquid states.

With no significant atomic mobility for structural change, an isostructural thermal expansion coefficient α_{th} is easily obtained from diffraction data below T_g . Also, the thermal expansion coefficient α_{th} may be measured by diffraction from the liquid state at various temperatures. Hence an “isochoric T_g ” [26–28] corresponding to the $\Delta\alpha_{th}$ difference between the glass below T_g and the supercooled liquid above T_g may in some cases be obtainable if significant experimental difficulties can be overcome.

Measurement of the “isochoric glass transition T_g ” by real-time diffraction was initially impossible as metallic glasses with crystallisation temperature T_x near T_g crystallised during real-time diffraction experiments. This limitation does not hold for newly developed bulk metallic glasses (BMGs) with large supercooled liquid regions $\Delta T \approx T_x - T_g$.

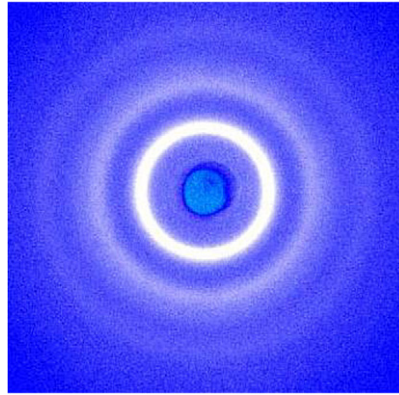


Fig. 1. Typical in-situ diffraction data of a glass obtained in transmission in the form of concentric rings much as in transmission electron microscopy. Radial integration of the rings yields the intensity $I(Q)$ versus wave-vector Q curves [29].

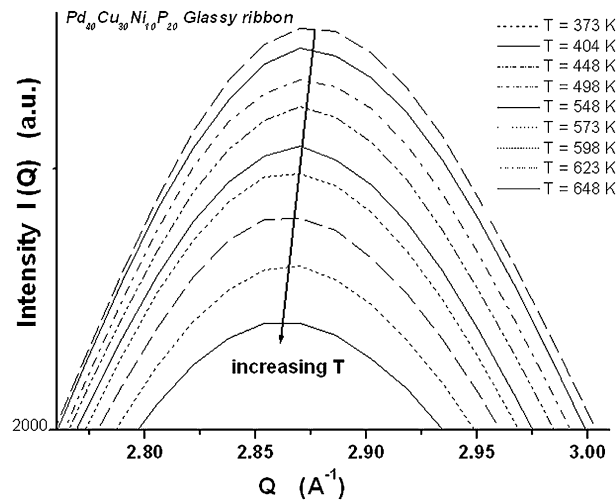


Fig. 2. Variation of Q_{\max} , the position of the maximum diffracted intensity $I(Q)$ with temperature as a result of thermal expansion [29].

Diffraction in transmission from a glassy structure typically yields patterns such as shown in the picture of Fig. 1 which is a screen image on the CCD camera. Here, the specimen is needle-shaped as cut from a bulk sample in order to fit into 1 mm diameter sealed capillary of a Linkam hot-stage in a monochromatised high-energy synchrotron beam [29]. The intensity patterns are concentric rings much as in transmission electron microscopy. Radial integration of the rings yields the intensity $I(Q)$ versus wave-vector Q curves.

As long as there is no significant change in the local atomic structures, the successive broad maxima of the diffraction patterns will move to lower Q values with increasing temperature (Fig. 2) as a result of thermal expansion and reversibly return to their initial Q_0 position upon cooling.

Precision measurements of the diffracted intensity $I(Q)$ versus wave-vector Q (reciprocal space) can yield real space atomic pair distribution functions via Fourier transformations as will be discussed later. But reversible effects of thermal dilatation can be obtained directly from diffraction data of metallic glasses in analogy to the shifting of Bragg peaks in crystalline materials [30]. In this approach, the variation with temperature of wave-vector Q_{\max} of the first diffracted intensity $I(Q_{\max})$ maximum will be inversely proportional to the mean atomic spacing (the Ehrenfest relation [31,32]). It would then follow that the third power of Q_{\max} will scale with the coefficient of volume thermal expansion of glassy structure as in:

$$\left\{ \frac{Q_{\max}(T_0)}{Q_{\max}(T)} \right\}^3 = \left\{ \frac{V(T)}{V(T_0)} \right\} = \{1 + \alpha_{th}(T - T_0)\} \quad (1)$$

where α_{th} is the volume coefficient of thermal expansion below T_g as long as no structural change occurs and corresponds to the temperature slope or derivative of the reduced mean atomic volume $\{V(T)/V(T_0)\}$ at T , with the reference T_0 corresponding to room temperature.

Subject to these conditions, the volume coefficient of thermal expansion at T_g was measured for a number of bulk metallic glasses. Clear variations of $\Delta\alpha_{th}$ were detected in the same glass transition temperature range (Figs. 3(b), 4(b)) as ΔC_p determined by calorimetry [24], see for example Figs. 3(a), 4(a). For these experiments, the heating and cooling rates

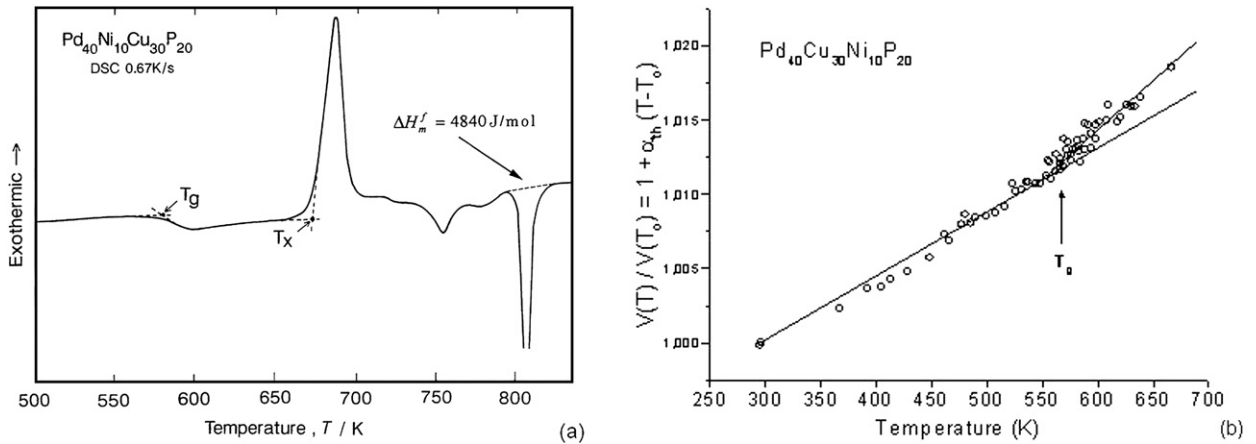


Fig. 3. Pd₄₀Cu₃₀Ni₁₀P₂₀ bulk metallic glass, (a) left: isentropic T_g determined calorimetry [24]; (b) right: isochoric T_g determined from diffraction data.

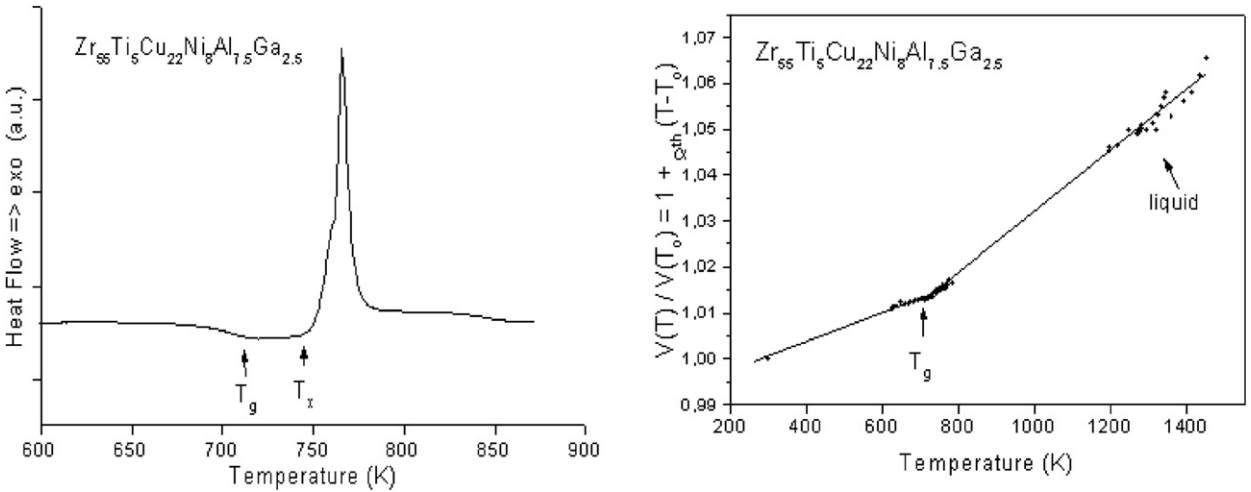


Fig. 4. Zr₅₅Ti₅Cu₂₂Ni₈Al_{7.5}Ga_{2.5} bulk metallic glass, (a) left: isentropic T_g determined calorimetry; (b) right: isochoric T_g determined from diffraction data.

of the Linkam hot stage in the beam were 10 K/min and calorimetric measurements were acquired at 40 K/min. While the measured T_g increases with heating rate, the expected increase with change from 10 to 40 K/min is less than 10 K for the onset of the transition.

It should be noted that while in the Ehrenfest relation leading to Eq. (1), “average atomic volume” V scales with (1/Q_{max})³ or Q_{max} scales with V^{0.33}, more recent results from Oak Ridge and comparison with measured mass densities indicate that Q_{max} in metallic glasses scales with V^{0.42} of a fractal structure rather than V^{0.33} of crystalline Bragg peaks [14].

From thermodynamics, while the first derivatives of the Gibbs free energy such as volume V change continuously across the glass transition, discontinuities in second derivatives such as the thermal expansion coefficient Δα_{th} and the isothermal compressibility Δκ_T should accompany ΔC_p, the three properties being related through various thermodynamic expressions [26]. According to Prigogine and Defay [34], the ratio $R = \Delta\kappa_T \cdot \Delta C_p / \{T V \cdot \Delta\alpha_{th}^2\}$ is expected to be equal to 1 independently of the order of the reaction provided that a single ordering parameter determines the position of equilibrium in a relaxing system and R > 1 if more than one ordering parameter is responsible. Once the discontinuities of the three second-order thermodynamic functions ΔC_p, Δα_{th} and Δκ_T have been determined with precision, the applicability of the constant R of Prigogine and Defay may be evaluated for the liquid–glass transition in metallic materials.

3. Measuring the “excess free-volume” ΔV_f in metallic glasses

In 1959, Cohen and Turnbull, using a “free-volume” formulation of viscosity, predicted that a metallic glass could be obtained if the melt was quenched fast enough to bypass crystal nucleation and growth [35]. The kinetics of diffusive atomic motion in a metallic glass can be modelled by including a dispersion of “holes” or “free volume” V_f in much the same way as “vacancies” or empty lattice sites control diffusive jumps of atoms in a crystal [36–41].

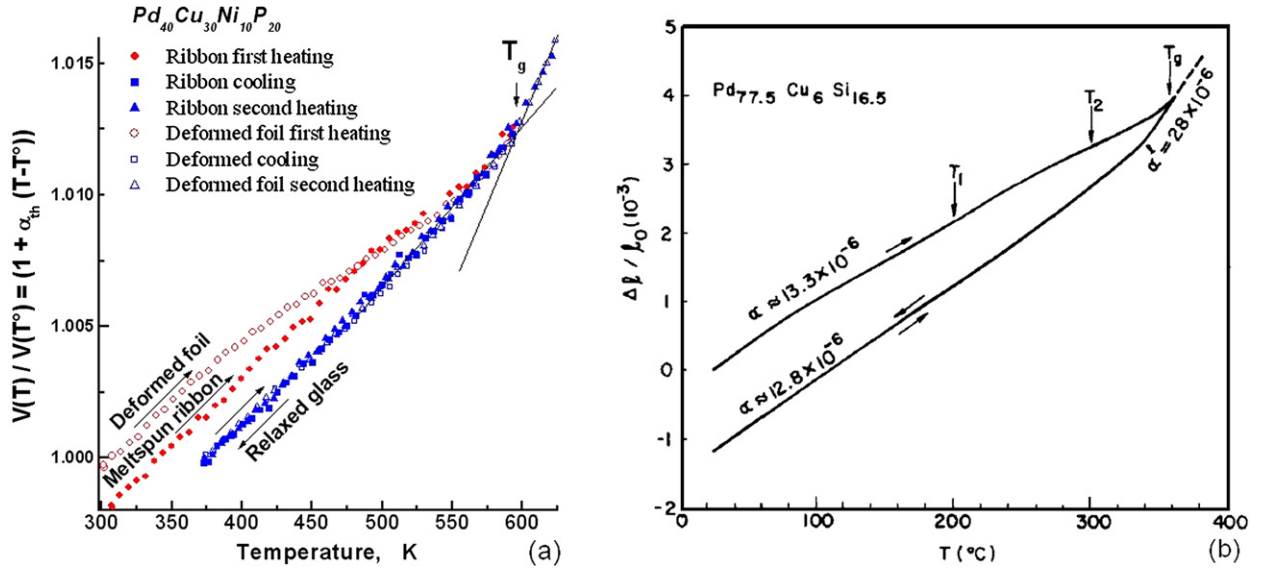


Fig. 5. (a): XRD volume per atom of Eq. (1) showing relaxation of both as-quenched ribbon and heavily deformed foils of the glass towards the same relaxed glassy state attained near T_g . Slope changes ($\Delta\alpha_{th}$) at T_g [29]. (b): Length change (dilatation) of a glassy Pd-based meltspun ribbon showing densification towards the relaxed glassy state attained near T_g . Slope changes ($\Delta\alpha_{th}$) at T_g [45].

At faster quench rates, excess free-volume ΔV_f can be trapped like excess vacancy content in quenched crystals.

In 1960, at the same time as the first metallic glasses were discovered, Simmons and Balluffi [30] devised experiments allowing precise determination of equilibrium lattice vacancies in crystals by simultaneously measuring the length change $\Delta L/L$ (by dilatometry) and lattice parameter change $\Delta a/a$ (by X-ray diffraction) with increasing temperature T . Their experiments which contributed to the quantitative understanding of point defects in solid-state physics [42] were based on the following simple equation for the vacant fraction of lattice sites C_v as a function of temperature T :

$$C_v(T) = 3 \left\{ \frac{\Delta L(T)}{L_0} - \frac{\Delta a(T)}{a_0} \right\} \quad (2)$$

where $\Delta a(T)/a_0 = \alpha_{th}^l(T) \cdot (T - T_0)/a_0$, L_0 and a_0 are the crystal length and lattice parameter at a reference temperature T_0 , and $\alpha_{th}^l(T)$ the linear coefficient of thermal expansion, itself weakly temperature-dependent [43]. Their experiments showed that C_v is nearly zero in a relaxed crystal at low temperatures but increases to tens and hundreds of ppm (less than 10^{-3}) as thermal vacancies are generated at high temperatures. To recapitulate, Simmons and Balluffi used the lattice parameter change $\Delta a(T)/a_0$ measured by X-ray diffraction to remove the part of the length-change due to the thermal expansion of the lattice. What remains of $\Delta L(T)/L_0$ then yields the increase in the vacant fraction of lattice sites.

If as in crystals, excess (quenched-in) free-volume in the glassy state took the form of atomic size holes, a combination of dilatation and X-ray diffraction measurements would be needed to determine V_f as for vacancies in crystals.

On the other hand, if as computer simulation predicted [44], atomic size holes or vacancies in a glass are unstable and the quenched-in free volume in liquids and glasses is randomly distributed, Eq. (2) of Simmons and Balluffi would not apply, $\Delta V(T)/V_0$ would be equal to $3\Delta L(T)/L_0$ and the mean atomic volume and the sample dimensions would evolve together with temperature.

Fig. 5(a) shows plots of Eq. (1) for rapidly solidified glassy $\text{Pd}_{40}\text{Cu}_{30}\text{Ni}_{10}\text{P}_{20}$ ribbon during thermal cycling at 10 K/min in a capillary on a Linkam hot stage in a monochromatised high energy synchrotron beam. Data is also reported for specimen after deformation which also generates excess free-volume [29].

It is seen that during initial heating the slope is constant with α_{th} about $5 \times 10^{-5} \text{ K}^{-1}$ or a linear coefficient of thermal expansion of $1.66 \times 10^{-5} \text{ K}^{-1}$ which is similar to values measured by dilatometry [46]. From about $T = 425 \text{ K}$ the plot dips until reaching $T_g = 570 \text{ K}$ at 10 K/min, just below the value determined by calorimetry at a higher heating rate of 40 K/min (Fig. 3(a)). A similar behaviour shown in Fig. 5(b) is observed in Pd-based glasses by dilatometry [45] when the apparatus is of the type that minimises stress on the specimen. Subsequent heating and cooling show only reversible dilatation and contraction with the same slope as the initial one indicating that the quenched state of the glass has densified to a fully relaxed state during heating to T_g . The volume difference between the initial as-quenched state (start of the first heating) and the subsequent relaxed state observed during T -cycling after heating to $T > T_g$ is about 0.2% which corresponds well to densification of melt-spun metallic glasses as measured by dilatometry [45] or creep measurements [47] and as discussed in terms of the free-volume interpretation of the glass-transition [48].

In Fig. 5(a), comparison with the deformed specimen highlights several interesting findings. Firstly, the difference between the first heating to $T > T_g$ and subsequent thermal cycling of the highly deformed foils corresponds to a densification

of about 0.4% of volume per atom. This indicates that heavy deformation (thickness reduction of 90 to 97%) has resulted in the generation of free-volume to a level double that of the same glass in the as-quenched state. This result is consistent with the generation of free-volume V_f during heterogeneous deformation of metallic glasses known to occur in shear bands also previously reported by dilatometric methods [45]. Secondly, the higher free-volume content in the deformed foils results in faster relaxation kinetics now detectable above 400 K. Perhaps most significantly, the relaxed states of the material after rapid quenching and after heavy deformation exhibit exactly the same volume with near constant thermal expansion and a break in α_{th} at T_g .

The fact that the average atomic volume in metallic glasses as deduced from X-ray diffraction scales with the macroscopic specimen dimensions (length change) as measured with dilatometry would thus correspond to $\Delta L(T)/L_0 = \Delta a(T)/a_0$ in the Simmons and Balluffi equation.

Synchrotron X-ray diffraction studies can also measure the kinetics of excess free-volume ΔV_f annihilation isothermally and determine activation energies [29]. These kinetics and activation energies are of interest for certain engineering applications such as shaping of springs without embrittlement [41].

4. In-situ vitrification and atomic structural features of supercooled Pd–Ni–Cu–P glass-forming liquid

Diffraction techniques applied to crystalline materials allow the identification of the periodic crystalline topology from the symmetry of the distribution of diffraction peaks in reciprocal space. The intensities of these Bragg peaks allow the determination of the atomic decoration of the crystalline lattices (chemical order). In this manner, phase transitions in the crystalline state can be precisely followed by diffraction data for the establishment of condensed-state equilibrium phase diagrams. Similarly, coherent scattering provided direct information on metastable ordered structures, texture, grain size, strains, effects of non-equilibrium processing (quench rate [49] and deformation [50,51]) on chemical ordering and superlattice formation as detected by appearance of superlattice Bragg peaks. This is not the case for metallic glasses and other amorphous materials which only produce successive broad diffraction halos that mask the effects of processing conditions on the distribution of coherent scattering in reciprocal space. Such information must then be searched for by analysis of atomic pair distribution functions in real space.

For this purpose, a glassy fluxed ingot of Pd_{42.5}Cu₃₀Ni_{7.5}P₂₀ [24] was encapsulated under secondary vacuum (of the order of 1×10^{-3} Pa) in a quartz container of 5 mm inner diameter. The sample was then heated in the beam by an induction heating method [33,52] to a temperature of 910 K, which is well above the liquidus temperature T_l and cooled down while the temperature was monitored by a pyrometer and the heater current calibration both normalised by known values of T_l , T_x and T_g . A continuous set of the data was obtained during cooling accelerated by a gas blower aimed at the container.

After correction for scattering from the sample container, air scattering, polarisation, absorption and Compton scattering the measured intensities were converted to electron units per atom $i(Q)$ with the generalised Krogh–Moe–Norman method using the X-ray atomic scattering factors and anomalous dispersion corrections. The total structure factor $S(Q)$ and the interference function $Qi(Q) = Q[S(Q) - 1]$, where $Q = 4\pi \sin\theta/\lambda$ and θ is the diffraction angle, were obtained from the coherent scattering intensity by using atomic scattering factors. The values of $Qi(Q)$ for $Q < 180 \text{ nm}^{-1}$ were smoothly extrapolated to $Q = 0$. The radial distribution RDF(r) and pair distribution functions PDF(r) were obtained by the Fourier transform of $Qi(Q)$:

$$\text{PDF}(r) = 4\pi r^2 \rho(r) = 4\pi r^2 \rho_0 + \frac{2r}{\pi} \int_0^{Q_{\max}} k Qi(Q) \sin(Qr) dQ \quad (3)$$

where $\rho(r)$ is the total radial number density function and ρ_0 is the average number density of the sample [53].

According to the XRD spectra, melting of the studied alloy during heating at 0.67 K/s starts at 780 K and the liquidus T_l is at around 800 K. After heating to above 900 K the sample was cooled at 8.33 K/s down to room temperature (298 K). The interference function $Qi(Q)$ at 298 K calculated from the XRD intensity profile after the described corrections is shown in Fig. 6. A typical atomic pair distribution functions PDF(r) obtained by the Fourier transform of $Qi(Q)$ is shown in Fig. 7.

As usual for glassy alloys, a detectable medium-range order is indicated by clear oscillations in PDF(r) which continue up to about 2 nm ([54] not shown here).

Obtaining continuous X-ray diffraction data in the supercooled liquid region between the liquidus T_l and the glass transition T_g temperatures is impossible for almost all glass-forming alloys because they crystallise during the time needed for acquisition of the successive spectra and to our knowledge, no other set of atomic pair distribution functions during vitrification from the liquid state are presently available. Broadly considered, the PDF(r) range presented in Fig. 7 shows that the 1st nearest neighbour (nn) coordination shell moves towards higher r and the 2nd coordination shell moves inwards on the r -scale during vitrification.

A shoulder at low r is visible on the 1st PDF (nn) peak and better seen on the expanded scale of Fig. 8 where the baseline was corrected prior to fitting as before [54]. At room temperature, the first sub-peak (P1) is likely due to increased number of metal–metaloid nearest neighbours while the main peak (P2) corresponds to larger metal atom pairs (Pd–Pd, Pd–(Ni–Cu)) of the majority components as expected from Goldschmidt atomic radii $r_{\text{Pd}} = 0.138 \text{ nm}$, $r_{\text{Cu}} = 0.128 \text{ nm}$, $r_{\text{Ni}} = 0.125 \text{ nm}$ and $r_{\text{P}} = 0.106 \text{ nm}$.

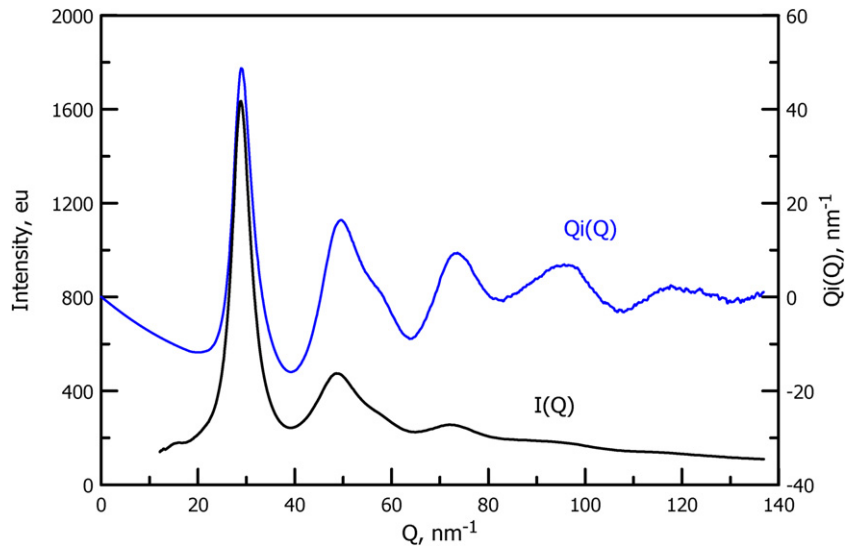


Fig. 6. The interference function $Q_i(Q)$ for glassy $\text{Pd}_{42.5}\text{Cu}_{30}\text{Ni}_{7.5}\text{P}_{20}$ at 298 K calculated from the XRD intensity after the necessary corrections [54].

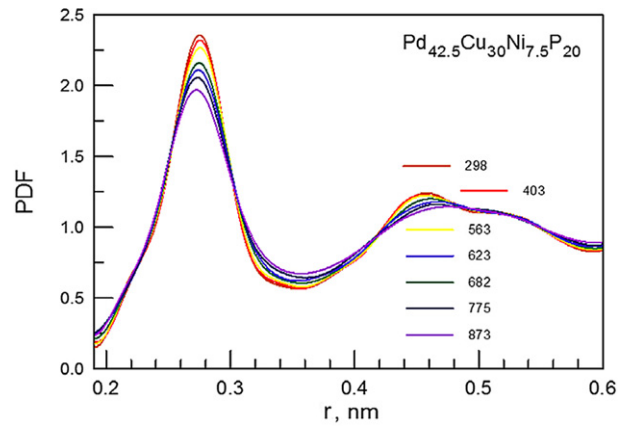


Fig. 7. PDF(r) functions of the studied alloy obtained at different temperatures in degrees Kelvin [54].

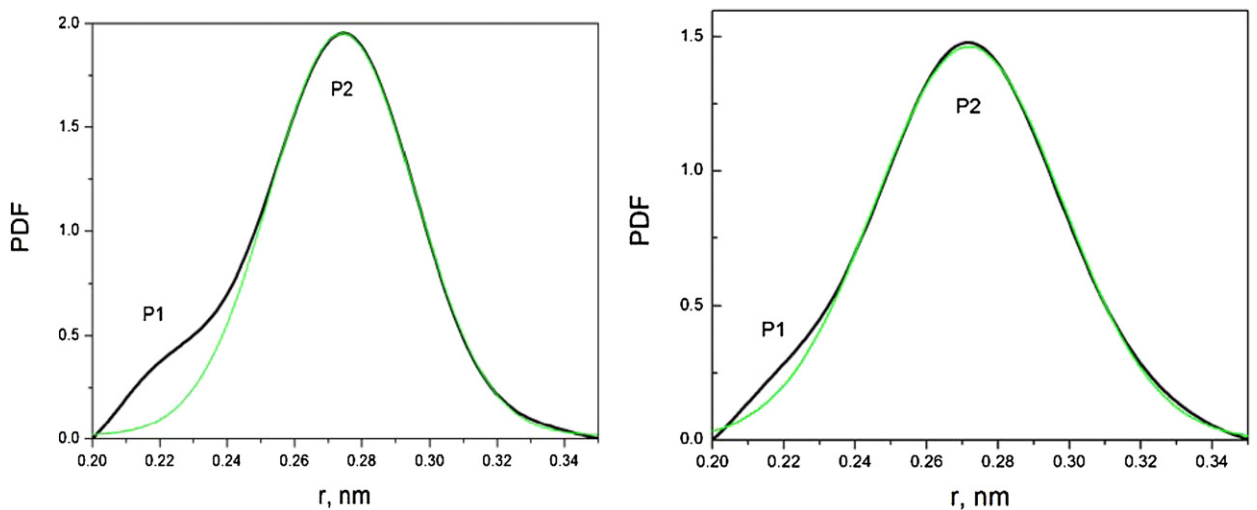


Fig. 8. Low temperature sub-peak P1 of the first PDF(r) maximum at 298 K (left) and 873 K (right). The Gaussian fit is only to guide the eye.

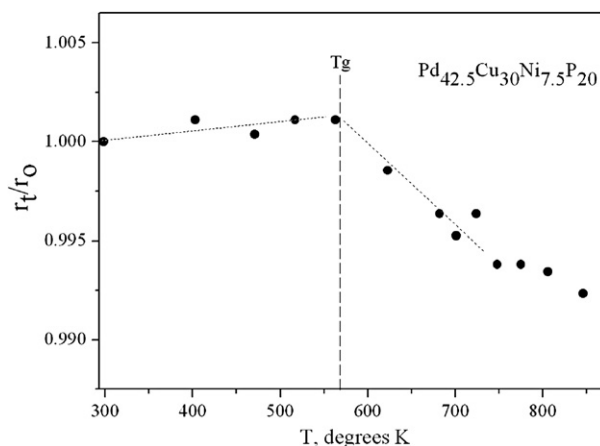


Fig. 9. Temperature dependence of the positions of the real-space 1st atomic coordination shell maximum, during cooling from the molten state with respect to its value at 298 K (dotted line are to guide the eye only).

Fig. 9 shows the shift of the position in real space r_T of the 1st nn coordination shell maximum as a function of temperature during cooling of the liquid alloy normalised to the room temperature value r_0 . It is seen that in the supercooled liquid temperature range below the liquidus $T_l > 800$ K, an increase in the nearest interatomic distances takes place on cooling while at lower temperature below the glass-transition $T_g \approx 580$ K, the interatomic distances begin to shrink.

The shift of the peaks on subsequent heating of the glassy sample was found to be similar. Of course a full set of data up to the liquidus is not available during heating as the latter's rate is slower than the cooling rate and the specimen crystallises before reaching T_l but detailed results in [54] indicate that the anomalous thermal expansion between T_l and T_g initially observed during vitrification of the liquid alloy is a reversible state property and thermodynamic in nature.

From the dilatation data of Figs. 3(b) and 1(a), the linear thermal expansion coefficient of the glassy state is about $1.6 \times 10^{-5} \text{ K}^{-1}$ and that of the supercooled liquid at $T > T_g$ is of the order of $5 \times 10^{-5} \text{ K}^{-1}$. Thus a linear thermal dilatation of about +2% is expected between 298 K and 898 K while the displacement of the maximum of the 1st nn shell in real space is about -2% mainly due to strong contraction between T_g and $T_g + 200$ K. There is no inherent contradiction between the observed contraction of the 1st nn shell in real space and the usual dilatation with increasing temperatures derived from reciprocal space because the latter is on a per atom basis and includes both the strong shift of the 2nd nn shell to larger r values and an increase of the number of atoms between the 1st and 2nd nn shell maxima with increasing temperature.

These results suggest the development of stronger compositional short-range order (CSRO) during cooling in the supercooled liquid from T_l to T_g . Phosphorous-metal atom interactions could be developing a more covalent character with increased (s, p)- d hybridisation.

5. Conclusions

In-situ vitrification in a synchrotron beam during cooling of the $\text{Pd}_{42.5}\text{Cu}_{30}\text{Ni}_{7.5}\text{P}_{20}$ melt has allowed continuous acquisition of X-ray diffraction spectra in the supercooled liquid region between the liquidus temperature T_l and the glass transition temperature T_g [29,33]. The experiments allowed precise determination of isochoric glass transitions and excess free-volume contents in metallic glasses.

More recent measurements during in-situ cooling (vitrification) and subsequent reheating allowed determination of structural changes in the supercooled and glassy states using real-space atomic pair PDF(r) and radial RDF(r) distribution functions. The nearest neighbour (nn) distance in the first coordination shell have a low r (distance) pre-peak that appears and grows on cooling from the liquidus temperature to the glass transition in the supercooled liquid region. A reversible expansion of the nn distances in the 1st coordination shell is observed in the same temperature range. This correlation is thought to be due to an increasing covalent character of the metal-metalloid bonding near T_g during cooling and a major contributor to the record glass-formability of PdCuNiP alloy family.

References

- [1] A. Inoue, *Acta Mater.* 48 (2000) 279.
- [2] A.H. Cottrell, *The Mechanical Properties of Matter*, John Wiley and Sons, 1964.
- [3] W.L. Johnson, K. Samwer, *Phys. Rev. Lett.* 95 (2005) 195501.
- [4] K. Georgarakis, M. Aljerf, Y. Li, A. LeMoulec, F. Charlot, A.R. Yavari, K. Chornokhostenko, E. Tabachnikova, G.A. Evangelakis, D.B. Miracle, A.L. Greer, T. Zhang, *Appl. Phys. Lett.* 93 (2008) 031907.
- [5] D.B. Miracle, A. Concustell, Y. Zhang, A.R. Yavari, A.L. Greer, *Acta Mater.* 59 (2011) 2831.
- [6] A.L. Greer, *Materials Today* 12 (2009) 14.

- [7] A.R. Yavari, J.J. Lewandowski, J. Eckert, *MRS Bull.* 32 (2007) 635.
- [8] A. Inoue, N. Nishiyama, *MRS Bull.* 32 (2007) 651.
- [9] W.L. Johnson, *MRS Bull.* 24 (1999) 42.
- [10] D.B. Miracle, *Nature Mat.* 3 (2004) 697.
- [11] A.R. Yavari, *Nature Mat.* 4 (2005) 2.
- [12] H.W. Sheng, W.K. Luo, F.M. Alamgir, J.M. Bai, E. Ma, *Nature* 439 (2006) 419.
- [13] A.R. Yavari, *Nature* 439 (2006) 405.
- [14] D. Ma, A.D. Stoica, X.-L. Wang, *Nature Mater.* 8 (2009) 30.
- [15] D.V. Louzguine-Luzgin, J. Antonowicz, K. Georgarakis, G. Vaughan, A.R. Yavari, A. Inoue, *J. Alloys Comp.* 466 (2008) 106.
- [16] A. Hirata, P. Guan, T. Fujita, Y. Hirotsu, A. Inoue, A.R. Yavari, T. Sakurai, M.W. Chen, *Nature Mater.* 10 (2011) 28.
- [17] J.D. Bernal, *Nature* 185 (1960) 68.
- [18] P. Desré, A.R. Yavari, P. Hicter, *Philos. Mag.* B 61 (1990) 1.
- [19] A.R. Yavari, *Phys. Lett. A* 95 (1983) 165.
- [20] W. Klement, R.H. Willens, P. Duwez, *Nature* 187 (1960) 869.
- [21] H.S. Chen, D. Turnbull, *Acta Mater.* 17 (1969) 1021.
- [22] D.E. Polk, D. Turnbull, *Acta Met.* 20 (1972) 493.
- [23] A.R. Yavari, A. Inoue, *Mater. Res. Soc. Symposium Proceedings* 554 (1999) 21.
- [24] N. Nishiyama, A. Inoue, *Acta Mater.* 47 (1999) 1487.
- [25] D. Turnbull, *Scientific American* 212 (1965) 38.
- [26] J. Jäckle, *Rep. Progr. Phys.* 49 (1986) 171.
- [27] J.L. Tallon, *Nature* 342 (1989) 568.
- [28] H.J. Fecht, W.L. Johnson, *Nature* 334 (1988) 59.
- [29] A.R. Yavari, A. Le Moulec, A. Inoue, N. Nishiyama, N. Lupu, E. Matsubara, W.J. Botta, G. Vaughan, M. Di Michiel, A. Kvick, *Acta Mater.* 53 (2005) 1611.
- [30] R. Simmons, R. Balluffi, *Phys. Rev.* 117 (1960) 52.
- [31] A. Guinier, *Théories et Techniques de la Radio-christallographie*, Dunod, 1964.
- [32] A.R. Yavari, *Acta Metall.* 36 (1988) 1863.
- [33] J.L. Uriarte, A.R. Yavari, N. Nishiyama, G. Heunen, G. Vaughan, Å. Kvick, A. Inoue, *Scripta Mater.* 48 (2003) 809.
- [34] S.R. Elliott, *Physics of Amorphous Materials*, John Wiley & Sons, New York, 1990, p. 35.
- [35] M.H. Cohen, D. Turnbull, *J. Chem. Phys.* 31 (1959) 1164.
- [36] F. Spaepen, *Acta Metall.* 25 (1977) 407.
- [37] A. Argon, *Acta Metall.* 27 (1979) 47.
- [38] A.R. Yavari, *J. Mater. Res.* 1 (1986) 746.
- [39] T.W. Wu, F. Spaepen, *Philos. Mag.* B 61 (1990) 739.
- [40] A.R. Yavari, *Mater. Sci. Eng.* 98 (1988) 491.
- [41] M. Aljerf, K. Georgarakis, A.R. Yavari, *Acta Mater.* 59 (2011) 3817.
- [42] A. Seeger, D. Schumacher, in: R.M.J. Cotterill, M. Doyama, J.J. Jackson, M. Meshii (Eds.), *Lattice Defects in Quenched Metals*, Academic Press, 1965, pp. 15–75.
- [43] P. Vinet, J.R. Smith, J. Ferrante, J.H. Rose, *Phys. Rev. B.* 35 (1987) 1945.
- [44] C.H. Bennett, P. Chaudhari, V. Moruzzi, P. Steinhardt, *Philos. Mag.* A 40 (1979) 485.
- [45] H.S. Chen, *J. Appl. Phys.* 49 (1978) 3289.
- [46] N. Nishiyama, M. Horino, A. Inoue, *Mater. Trans. JIM* 41 (2000) 1432.
- [47] A.I. Taub, F. Spaepen, *Acta Metall. Mater.* 28 (1980) 1781.
- [48] A. Van Den Buekel, J. Sietsma, *Acta Metall. Mater.* 38 (1990) 383.
- [49] A.R. Yavari, B. Bochu, *Philos. Mag.* A 59 (1989) 697.
- [50] T. Benameur, A.R. Yavari, *J. Mater. Res.* 7 (1992) 2971.
- [51] A.R. Yavari, *Acta Metall. Mater.* 41 (1993) 1391.
- [52] A.R. Yavari, A. Le Moulec, A. Inoue, F. Walter, J. Botta, G. Vaughan, A. Kvick, *Mat. Sci. Eng.* A 304–306 (2001) 34.
- [53] Y. Waseda, *The Structure of Non-Crystalline Materials*, McGraw-Hill, New York, 1980, p. 670.
- [54] K. Georgarakis, D.V. Louzguine, J. Antonowicz, G. Vaughan, A.R. Yavari, T. Egami, A. Inoue, *Acta Mater.* 59 (2011) 708.